**Showcasing the perspective from the groups of
Prof. Shuichi Hiraoka at the University of Tokyo,
Dr Satoru Iuchi at Nagoya University, and
Prof. Hirofumi Sato at Kyoto University, Japan.**

Theoretical and computational methodologies for
understanding coordination self-assembly complexes

Three methods to capture the coordination self-assembly
processes at the molecular level are highlighted: quantum
chemical modeling, molecular dynamics, and reaction
network analysis, covering different scales from the
metal–ligand bond to a more global reaction network
theoretically and computationally. Suitable numerical
approaches to analyze the coordination self-assembly
from different perspectives are introduced. Studies
based on these methods are paving the way to
elucidate increasingly more aspects of the coordination
self-assembly.

As featured in:

See Satoshi Takahashi,
Hirofumi Sato *et al.*,
Phys. Chem. Chem. Phys.,
2023, **25**, 14659.

**ROYAL SOCIETY
OF CHEMISTRY**

rsc.li/pccp

PERSPECTIVE

Check for updates

Theoretical and computational methodologies for understanding coordination self-assembly complexes

Satoshi Takahashi, [iD] *[a] Satoru Iuchi, [iD] [b] Shuichi Hiraoka [iD] [a] and Hirofumi Sato [iD] *[cd]

This perspective highlights three theoretical and computational methods to capture the coordination self-assembly processes at the molecular level: quantum chemical modeling, molecular dynamics, and reaction network analysis. These methods cover the different scales from the metal–ligand bond to a more global aspect, and approaches that are best suited to understand the coordination self-assembly from different perspectives are introduced. Theoretical and numerical researches based on these methods are not merely ways of interpreting the experimental studies but complementary to them.

1 Introduction

Molecular self-assembly is a chemical process in which constituent units become spontaneously arranged structures based on intermolecular interactions.[1–4] It is one of the most fundamental strategies for imparting function to materials in biological and artificial systems. From the nanoscale to the macroscale, many structures that support life are built by molecular self-assembly. In other words, life has been constructed by highly complex chemical systems based on the fundamental principle of molecular self-assembly, which has evolved over many years. Understanding the fundamental rule governing artificial systems is also vital in applying molecular self-assembly to materials science which has also made significant progress over the past several decades. Here in this article, we report theoretical and numerical methodologies on the discrete coordination self-assembly complexes, which consists of organic multitopic ligands (L) and metal ions (M), with the contributions of the present authors being highlighted. One of the reasons why the coordination self-assembly is focused on is that bonding patterns between the building blocks and the resultant structures of the products are well-defined compared to other artificial or biological self-assembly systems due to the

coordination number and direction of the metal being strictly fixed. We believe that the insights obtained through the studies introduced in this paper are available in other molecular self-assembly systems.
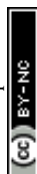
As a matter of course, the research of molecular self-assembly had been led by experimental studies. However, as the interests and concerns are getting directed not only to the final products but also to the global reaction process, the situations and approaches should change in order to track the reaction pathways and obtain the information about dominant elementary reactions, rate-determining steps, kinetic traps, *etc.* Even with the state-of-the-art experimental techniques, it is very difficult (practically impossible) to observe all the intermediate species transiently produced in the course of the self-assembly. The past experimental studies explicitly associated with the reaction process were limited to the self-assembly systems in which long-lived intermediate species could be experimentally observed. However, as will be exemplified later, it is not clear whether these long-lived species are really on the main reaction pathway or not, because those species too rapidly converting to the next intermediates cannot be observed experimentally even if those are on the main pathway. Additionally, it is not possible to determine with experiments alone what kind of microscopic behavior is occurring at the level of electronic states in leading to the final assembly product. Therefore, it is natural that a different approach, which is not only a mere follow-up tool but also hopefully supportive, should be taken to obtain more reaction details, with theoretical/computational tools appearing as the most suitable candidates. Another advantage arising from experimental research going hand in hand with theoretical research is that the laborious and costly experimental manipulations, material and experimental designs that must

[a] *Department of Basic Science, Graduate School of Arts and Sciences, The University of Tokyo, 3-8-1 Komaba, Meguro-ku, Tokyo 153-8902, Japan. E-mail: ghnr5571@g.ecc.u-tokyo.ac.jp*

[b] *Graduate School of Informatics, Nagoya University, Furo-cho, Chikusa-ku, Nagoya 464-8601, Japan*

[c] *Department of Molecular Engineering, Kyoto University, Nishikyo-ku, Kyoto 615-8510, Japan. E-mail: hirofumi@moleng.kyoto-u.ac.jp*

[d] *Fukui Institute for Fundamental Chemistry, Kyoto University, Sakyo-ku, Kyoto 606-8103, Japan*

This journal is © the Owner Societies 2023

Phys. Chem. Chem. Phys., 2023, **25**, 14659–14671 | **14659**

be performed to reach the desired results can be minimized with the help of theoretical predictions.

From theoretical and computational points of view, the well-arranged, final geometrical structure is thought to be determined as the free energy minima of the system's potential (or free) energy hypersurface. Hence, two aspects are critical to the understanding of the process. One is how to evaluate the surface, and the other is how the system develops on the surface. Namely, these two may be considered to focus on local and global aspects of the surface. For the former, accurate computation of the formation energy is a primary concern. In particular, bond formation between M–L is the key because the interaction requires the quantum chemical description. Although multi-configuration *ab initio* theory such as CASSCF might be needed to adequately describe the electronic structure of coordination self-assembly complexes, widely used density functional theory (DFT) could be a more reasonable choice because of its handiness and computational costs. However, it should be pointed out that because many isomers and inter-mediates exist in an assembly process, more rapid computations are necessary to sufficiently explore a wide area of the surface to grasp the landscape of the energy surface.[5,6] Using classical-type potential, such as molecular mechanics (MM), is sufficiently cheap in computations but the treatment of M–L bond is usually infeasible due to the lack of quantum mechanical description, especially a proper consideration of d-electrons.[7] For the latter, the idea of reaction pathways embedded in a complex reaction network is inevitably related to the concept of the energy landscape. That is, expected chemical species or microstates like conformers are located at the local minima of the energy land-scape and reactions indicating the events of overcoming transition states are connecting those local minima. In this view, a well-defined kinetically controlled reaction pathway can be created by suitably modulating the corresponding energy landscape in some manners. There are some pioneering previous studies, for example, treating self-assembly pathways from the point of view of the energy landscape[8] or showing the dynamical simulations of such processes.[9] Putting the energy landscapes perspective in the context of the present article, products obtained through efficient molecular self-assembly requires the global energy landscape to have a single funnel, giving a well-defined minimum value of the free energy.[10–12] Many such processes proceeding under thermo-dynamic control are interested in the yield of final products, and understanding the details of reaction pathways are considered to have nothing to do with both the preparation and the result of experiments. But in reality, the knowledge of reaction pathway details largely helps to rationally control the yield of the products under the kinetic control by modulating the energy landscape.

The present article is organized as follows. In the next section, we show some quantum chemical approaches for the coordination self-assembly, to abstract the reaction mechanism *via* the most fundamental level in molecular theory, that is, the electronic structure. In Section 3, researches that adopted the molecular dynamics (MD) simulations as the way to directly track the global process of the self-assembly are introduced. As another way for tracking the global process of the self-assembly

from a panoramic point of view, Section 4 introduces kinetic studies based on the stochastic algorithm. Finally, we conclude this paper with an outlook.
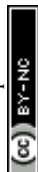
2 Quantum chemical approach

To reveal structural details of coordination self-assembly systems, the directional coordination bonds, which are the key to the metal-complex formation, have to be described appropriately at the atomic level. The directionality of M–L bonds originates from the effects of metal d-electrons and thus incorporating the d-electron effects is the key to computational methods. In this section, various computational methods are briefly outlined in terms of the description of the directional coordination bonds. Then, quantum mechanical modelings to include the d-electron effects are focused with emphasis on their concepts. Finally, applications of the aforementioned computational methods are outlined in terms of computations on structural characteristics of metal-containing systems. Note that various computational methods are comprehensively reviewed for metallo-organic cages with broader perspectives in other literatures.[5,6]

2.1 Brief overview of various computational approaches

In terms of computational costs, MM is one of the most attractive approaches to explore large molecular structures including self-assembly systems. However, the MM force fields are not based on quantum mechanical description and do not include the d-electron effects explicitly. By contrast, *ab initio* electronic structure and DFT methods naturally describe the directional coordination bonds by construction. In particular, the wavefunction-based *ab initio* approaches such as the multi-reference perturbation methods include the electron correla-tion effects, which are important for metal containing systems, with high accuracy. However, the computational costs become problematic for large metal containing systems. On the other hand, DFT calculations provide reasonably accurate results with less computational costs for metal containing systems. In this respect, the first-principle DFT calculation is an approach suitable for computations of large metal containing systems including coordination self-assembly. The tight-binding DFT method, which is a semiempirical method, has also attracted interest in applica-tions to metal-containing systems.[13,14]

Several quantum mechanical approaches have been also developed to include the d-electron effects. The electronic structures of transition metal complexes have been often inter-preted by the crystal field (CF) or ligand field (LF) theories, where the electronic d–d states arising from the $(nd)^{N_d}$ config-urations with N_d being the number of d-electrons are described by the CF or LF contributions and the repulsions between the d-electrons.[15] In the CF or LF pictures, the metal d-orbitals are split in energy due to the field on the metal ion created by surrounding ligands. An approach to incorporate such LF contributions (the d-orbital splittings) into force fields has been developed.[7] On the other hand, an effective model Hamiltonian approach has been developed to incorporate both the M–L

14660 | *Phys. Chem. Chem. Phys.*, 2023, **25**, 14659–14671

This journal is © the Owner Societies 2023

interactions and the d-electron repulsions explicitly, with having wavefunctions in a d-orbital space.[16,17] A more rigorous effective Hamiltonian approach named the effective Hamiltonian crystal field (EHCF) method[18,19] has been developed to describe d–d states of transition metal containing systems. In the next section, these quantum mechanical approaches for metal containing systems are focused with emphasis on their concepts.

2.2 Quantum mechanical methods to incorporate d-electron effects

In the LF picture, the d orbital energies can be computed by the diagonalization of the 5×5 ligand field matrix $\boldsymbol{V}_{LF}$, composing of the one-electron matrix elements, $\langle d_i | \hat{v}_{LF} | d_j \rangle$.[15] In the CF picture, surrounding ligands are simply modeled by charges and $\hat{v}_{LF}$ is described only by the electrostatic contribution. However, the M–L bonds include covalent character to some extent, and the interactions between the metal d and ligand orbitals should be considered. The angular overlap model (AOM) describes the d-orbital splittings by parametrizing the M–L orbital interactions of M–L bond.[15,20] Because the orbital interactions are connected with the overlap integrals between the metal d and ligand orbitals, the total LF effects are given as a sum of the individual M–L bond contributions as[7]

$$\langle d_i | \hat{V}_{LF} | d_j \rangle = \sum_l^{M-L} \sum_k^{\sigma,\pi} F_{ik}^l F_{jk}^l e_k^l, \qquad (1)$$

where F represents the angular contributions and the radial contributions $e_{\sigma,\pi}$ are the parameters representing σ and π type interactions. The ligand field stabilization energy (LFSE) is given as the sum of the d-orbital energies weighted by appropriate occupation numbers of these d-orbitals. In the so-called LFMM and relevant approaches,[7] the LFSE is added into force fields. Therefore, these approaches can include the d-electron effects explicitly and the directionality of coordination bonds is taken into account through the AOM treatment. However, the electronic characters of transition metal complexes such as the spin multiplicity of the ground state are determined by a balance between the LF stabilization and the d-electron repulsions. In the LFMM approach, the d-electron repulsions are not included explicitly, and computations of relative energies between different spin states are not automatic and additional pragmatic parameterizations are necessary.[7]

On the other hand, the Hamiltonian matrix including both the LF contributions and the d-electron repulsions on the basis of $(nd)^{N_d}$ configurations could automatically include the information on multiple electronic states. As such an approach, we have been developing a model effective Hamiltonian which can describe the d–d states of the central metal ion under the influence of surrounding ligands.[16,17] In this approach, the electronic energy E_m and the wavefunction Ψ_m for the mth d–d state at a given nuclear configuration $\boldsymbol{R}$ are computed by diagonalizing the model Hamiltonian matrix as

$$\boldsymbol{H}_{model}(\boldsymbol{R})C_m(\boldsymbol{R}) = E_m(\boldsymbol{R})C_m(\boldsymbol{R}) \qquad (2)$$

and

$$|\Psi_m(\boldsymbol{r}; \boldsymbol{R})\rangle = \sum_{I=1}^{N_{config}} C_{Im}(\boldsymbol{R})|\Phi_I(\boldsymbol{r}; \boldsymbol{R})\rangle, \qquad (3)$$

where $\boldsymbol{r}$ represent the electronic coordinates and Φ are the Slater determinants representing the $(nd)^{N_d}$ configurations. For example, the number of such configurations, N_{config}, is 45 arising from the $(4d)^8$ configurations for a Pd(II) complex. In this modeling, all Φ are composed of only the metal nd atomic orbitals, and the ligands are represented by force fields. In this framework, the d-electron effects are naturally incorporated through a linear combination of various configurations as in eqn (3). All the d–d states are computed at the same time, meaning that not only the relative energies between the different spin states but also the d–d excitation energies are automatically computed.

The key of the above model Hamiltonian is the proper modeling of the $\boldsymbol{H}_{model}$ matrix elements. Because only the metal d–d states are concerned, the $(nd)^{N_d}$ configurations with the ground state configuration of the ligands are primarily considered (P space). The ligand-to-metal charge-transferred configurations are considered as the other space (Q space). By this space division, an effective Hamiltonian $\boldsymbol{H}_{eff}$ for the P space under the influence of the Q space is derived. Then, appropriate forms of the $\boldsymbol{H}_{model}$ matrix elements are determined through chemically intuitive arguments with the aid of $\boldsymbol{H}_{eff}$. By considering the nature of the P and Q spaces, the M–L electrostatic (ES) and exchange (EX) interactions are derived from the term only containing P space and the M–L charge transfer (CT) interaction is derived from the term containing the Q space. Therefore, the matrix elements are modeled as the sum of various M–L interaction related parts:

$$(\boldsymbol{H}_{model})_{IJ} = H_{IJ}^M + H_{IJ}^{ES} + H_{IJ}^{EX} + H_{IJ}^{CT}. \qquad (4)$$

The first matrix elements (M) describe the d-electron repulsions within the isolated metal. The ES matrix elements contain $\langle d_i | \hat{v} | d_j \rangle$, where $\hat{v}$ is the electrostatic potential by the ligand charges. Similar to AOM, the EX and CT matrix elements are modeled by the appropriate overlap integrals between the d and ligand model orbitals. Several adjustable parameters employed in these matrix elements are determined so that the model Hamiltonian reasonably reproduces reference *ab initio* electronic structure and/or DFT calculation results. For example, the MCQDPT and DFT methods were chosen to obtain reference calculation results in ref. 16 and 17, respectively. Therefore, the model Hamiltonian could be an alternative of *ab initio* electronic structure and/or DFT calculations.

In the above model Hamiltonian approach, the effective Hamiltonian is derived in a simplified fashion for the use in modeling the Hamiltonian matrix elements. In the EHCF method,[18,19,21,22] an effective Hamiltonian for transition metal containing systems is derived in a more rigorous fashion. In the *ab initio* electronic structure calculations, the electron correlation effects can be described by taking account of all the electronic configurations including metal and ligands.

This journal is © the Owner Societies 2023

Phys. Chem. Chem. Phys., 2023, **25**, 14659–14671 | **14661**

However, such full configuration interaction (CI) approach is infeasible in practice due to the computational costs. In the EHCF method, by dividing the valence orbitals of transition metal and ligand atoms into the d and l subsystems, the Hamiltonians for two subsystems are derived. As a result, a hybrid approach is realized in which only the d subsystem is deal with the $(nd)^{N_d}$ configurations. In this way, the d–d states are computed by the effective Hamiltonian of the d subsystem incorporating the effects from the l subsystem.

2.3 Applications of various approaches

In this subsection, applications of the aforementioned approaches are outlined in the same order as in Section 2.1. Note that applications to metal-containing systems other than the self-assembly ones are also included here.

One of the drawbacks of force fields is the lack of transferability to arbitrary molecular systems because they are not based on quantum mechanical description. In fact, various force fields have been developed for limited class of systems, and there are various efforts to construct force fields specialized for metal containing systems.[23] For example, in the cationic dummy atom (CaDA) model, the M–L electrostatic interactions are described by using the dummy charges placed around a metal ion to express the directionality of the M–L bonds. Several applications of this model to self-assembly systems are described in Section 3. On the other hand, a generic force field named GFN-FF[24] has been developed to achieve fast structure optimizations for various chemical systems. It was shown that the GFN-FF optimized structures of metal–organic porous materials such as $Pd_{46}L_{96}(BF_4)_{96}$ agrees with the experimental crystal structures.[24]

As for the electronic structure theory calculations, the DFT calculations have been widely utilized for coordination self-assembly systems by considering the accuracy and computational costs. Efforts to improve DFT methods have been continuing for more accurate description of structural properties of large molecular systems, difficult to be explored by the wavefunction based *ab initio* methods such as CASSCF/CASPT2. The B97-3c composite method[25] is an example, which has been tested for small molecule binding in metal–organic frameworks (MOFs) and porous organic cages.[26] However, even the DFT methods have limitations on the system size due to their computational costs. Accurate tight binding DFTs, called GFNn-xTB, have been developed for the calculation of structures of large molecular systems[13,14] and the applications include the structure optimization of the self-assembled $[Pd_{12}L_{24}]^{24+}$.[13] The GFNn-xTB method with the GBSA implicit solvation model has also applied to the structure optimizations of large metal complexes including self-assembly systems such as $Pd_{30}L_{60}(BF_4)_{60}$.[27]

The structures of transition metal complexes are often affected by electronic effects arising from various $(nd)^{N_d}$ electronic configurations, which are irrelevant to organic systems. The LFMM method is based on a quantum mechanical modeling and has successfully described these structural characteristics.[7] For example, the LFMM method generated distorted structures of various $Cu(\text{II})N_6$ complexes which agree with experimental data.[28]

The structures could be different when the spin multiplicities are different, which has been also modeled by the LFMM.[29,30] The LFMM method was also applied to simulating the CO_2-induced flexibility of a flexible MOF[31] and spin-crossover behavior in a MOF.[32] In the LF theory, the LF effects and the d-electron repulsions have been regarded as parameters, extracted from experimental data on d–d spectra. In the LFMM case, the LF stabilizations are determined by the AOM parameters as shown in eqn (1). On the other hand, the quantum chemical methods to extract the LF related parameters have been proposed based on DFT[33] and CASSCF and NEVPT2 calculations.[34] *Ab initio* LFT (AILFT) becomes a tool to extract the LF parameters and the d-electron repulsions from such and related *ab initio* calculations.[34,35] An approach to automate the fitting procedure to determine the AOM parameters has been also proposed by utilizing the AILFT.[36]

The aforementioned model effective Hamiltonian approach[16,17] can describe the electronic d–d states by construction, so the structural characteristics arising from electronic effects are naturally incorporated. In fact, the model Hamiltonian could be constructed for a spin-crossover $[Fe(2,2'-\text{bipyridine})_3]^{2+}$ complex based on the DFT calculations, where the high-spin quintet structure is more expanded than the low-spin singlet ground state one.[17] The model Hamiltonian approach was also applied to a ligand exchange reaction of $[PdPy_4]^{2+}$ with free pyridine (Py).[37] The potential energy profile of this reaction was adequately reproduced compared to *ab initio* MP2 calculation results, indicating that the change of ligand environment during the reaction is properly described through the change of weights of $(4d)^8$ electronic configurations. This model Hamiltonian was further applied to investigate the chiral effects on the final step of $[Pd_6L_8]^{12+}$ self-assembly.[38] In addition, the model Hamiltonian for a metal center was applied to compute the structures of a self-assembled nanocage $[Pd_{12}L_{24}]^{24+}$ and its partial series $[Pd_nL_m]^{2n+}$ in gas and solution phases, where the solvation was treated implicitly by the GB model.[39] Fig. 1 shows a performance of the model Hamiltonian in terms of single-point binding energies of $[Pd_nL_m]^{2n+}$, where a good agreement with the DFT results clearly indicates the reliability of the model Hamiltonian approach. A metal center is separated spatially from the other metal centers, so the other metal centers are reasonably modeled by partial charges, indicating that the model Hamiltonian for each metal center is diagonalized under the influence of all ligands and the other metal ions. The ground state energy of a coordination self-assembly was thus computed by using a sum of the electronic energies of the multiple metal centers, realizing efficient computations on structures of the Pd-based self-assembled systems.[37–39]

The EHCF method, which also describes the electronic d–d states by construction, has been applied to computing structures and d–d excitations of wider range of transition metal complexes.[18,19,21] For example, the EHCF approach combined with MM could successfully reproduce the structures and spin states of a wide range of Fe(II) and Co(II) complexes having mono- and poly-dentate nitrogen donor ligands.[19,21] The EHCF has been also extended to periodic solids by incorporating effects from band structures, which was tested for the periodic transition metal oxides such as MnO.[22]
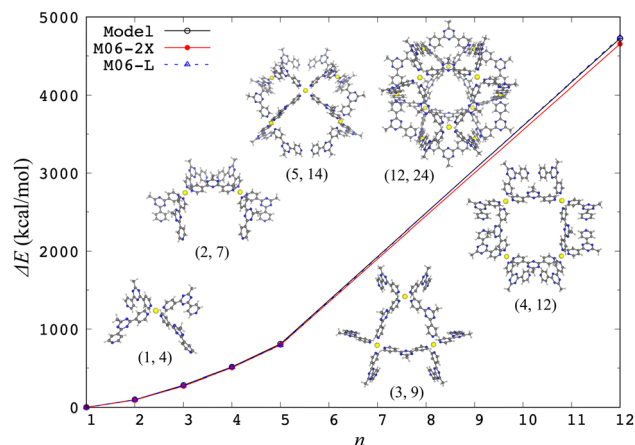
14662 | *Phys. Chem. Chem. Phys.*, 2023, **25**, 14659–14671

This journal is © the Owner Societies 2023

Fig. 1 Single-point binding energies ΔE from the model Hamiltonian and the DFT calculations with two different functionals, where $\Delta E = E(Pd_nL_m) + (4n - m)E(L) - nE(PdL_4)$ at the crystal $[Pd_{12}L_{24}]^{24+}$ and its partial $[Pd_nL_m]^{2n+}$ structures. Reproduced from Y. Yoshida, *et al. Phys. Chem. Chem. Phys.*, 2021, **23**, 866–877.[39]

3 Molecular dynamics

The relationship between complex reaction networks and energy landscapes has long been the subject of theoretical studies for structure prediction and extraction of molecular properties.[40,41] Kinetic transition network[12,42,43] provides a comprehensive description of transition processes and allows interpretation of molecular behaviors based on the energy landscape features. This is obtained as a mapping of the energy landscape or *via* MD data, with nodes and edges on the network corresponding to local minima and the transitions connecting them, respectively. This coarse-grained (CG) representation is very useful as a complementary approach to Monte Carlo and MD simulations. Visualization of the network is explicitly realized by using the so-called disconnectivity graph. This facilitates understanding the relationship between local minima, which are the lower ends of lines connected to each other at the lowest energy points (transition states).[44,45] Based on this framework, thermodynamics and kinetics have been extensively discussed from atomic and molecular clusters,[46,47] to CG models with rigid body components,[48–50] condensed matter systems,[51] biophysical systems,[52,53] and of course assembly processes.[54] Reaction rate constants can be calculated from conventionally used methods such as transition state theory, unimolecular kinetics, and direct dynamics calculations. Methodological and technical improvements in the kinetic transition network approach[55–57] to extracting thermodynamic and kinetic properties can be incorporated into other methodological frameworks for the reaction network-based analysis.

In the attempts to understand the self-assembly events, if it is possible to directly track and reproduce the global reaction process in computers, formation process of a certain geometrical structure can be visually captured. MD simulations would be adopted as the best way to such a purpose. In spite of the long and steady methodological development, MD studies on the coordination self-assembly started only recently, with

one of the pioneering works published by Yoneya and co-workers in 2012.[58] They selected an M_6L_8 nanosphere as a target system and demonstrated that over the course of simulations the spontaneous formation of the final product could be successfully observed.

To track the formation process of a nanosphere of octahedral symmetry composed of six Pd(II) ions and eight tritopic ligands, they specifically took the following procedures: (i) CaDA model was applied, in which four identical dummy atoms are coplanary attached to the Pd(II) ions. In this model the atomic charge of the Pd(II) cation is transferred to those four dummy atoms. Although the M–L binding in this model is purely electrostatic and too simple to represent the reality, in this study the simulation was performed with this model to propose the minimum model for the M_6L_8 self-assembly. (ii) A flexible united-atom model was applied for the tritopic ligand, with the exception of all the bonds being fixed to those at the equilibrium. (iii) They treat the solvent implicitly as a continuum medium to accelerate the assembly of metals and ligands to fill the time scale gap between the simulation and the reality. The combination of the Langevin dynamics (dynamic effects of the solvent molecules are taken into account), reaction fields (electrostatic effects of the solvent is represented by extending the classic reaction field method to ionic systems), and CG potentials (for van der Waals potential between ligands to be effectively short-range repulsive) was applied. It was found that the simulation results correlate well with the corresponding experimental ones, and that the difference in the lifetime between small-sized incomplete clusters and the completed M_6L_8 complex is crucially important in this self-assembly.

Subsequently, Yoneya and co-workers performed MD simulations and demonstrated the spontaneous formation for a $M_{12}L_{24}$ spherical complex.[59] One of the contrast to the M_6L_8 is that they found the existence of kinetic traps with lower number of metal nuclei such as M_6L_{12}, M_8L_{16}, and M_9L_{18}. Their study made it clear that it is important to consider the kinetic factor in the self-assembly process of the larger complex. Behaviors of kinetic traps are strongly dependent on the bend angle of the ligand and the M–L bonding strength. It should be noted that the self-assembly processes identified in their simulations are used as a reference for running even larger MD simulations.[60]

Motivated by the above pioneering studies, and highlighting the importance of the function of the self-assembled structure as a molecular container, Jiang *et al.* presented an MD simulation to investigate the encapsulation of C_{60} and C_{70} fullerenes during the self-assembly process of a M_2L_4 nanocapsule that is self-assembled by the coordination of Hg cations and bent ditopic ligands.[61] Stepwise formation of the nanocapsule and competitive fullerene encapsulation during dynamic structural changes in the self-assembly were detected successfully. This work helps design new functional nanomaterials capable of guest encapsulation and release.

Here we briefly mention the MD simulations for MOF or PCP (porous coordination polymer) and the nanocube, by viewing them as analogous systems in the context of tracking the

This journal is © the Owner Societies 2023

Phys. Chem. Chem. Phys., 2023, **25**, 14659–14671 | **14663**

molecular self-assembly process. In the MOF structure, vertices composed of single metal ions or ion clusters are linked by organic ligands. MOF is an important class of nanoporous materials because of its structural and functional properties, including the catalytic activity and the abilities for energy and gas storage. On the establishment of the design strategies for this artificial material, especially in mimicking the high-efficiency natural counterparts, a well-suited design of both the metal ion and the ligand is highly required. Although there are only a few works performed for obtaining the information about the growth process, knowing the details of (self-)organization processes and their mutual relations in time and space of various levels are getting more and more important. In a pioneering MD simulation for the growth process of MOF,[62] the model developed for the MD study of the $Pd_{12}L_{24}$ complex was applied to MOF, by using the CaDA and the CG solvent models. Self-assembly simulations for the two- and three-dimensional MOFs were performed by modeling the M–L bond with the Coulomb potential. The simulation of the two-dimensional MOF self-assembly led to the identification of the range of the dielectric constant in the near-field to achieve regular networks. For the three-dimensional case, they tried to reveal the design factor for realizing regular 3D MOF. By keeping in mind the uncertainty of how the self-assembly process is affected by the continuum solvent model, Biswal et al. conducted systematic and comprehensive researches on the MOF self-assembly having Zn ion. In one study,[63] they considered the models with different system size and the solvent types, succeeded the assembly of several two-dimensional layered network-like square arrangements, characterized the multistep assembly processes, and identified different geometrical structure of transient intermediates. In the other work,[64] model-dependence of the structural behaviors in the self-assembly process was examined on the different Zn-ion, solvent, and ligand models. From their exhaustive analysis it was found that the model should be carefully chosen in the research of the MOF self-assembly.

Nanocube is a hexameric self-assembled structure of six gear-shaped amphiphile molecule, and it has about 1 nm-sized inner space, in which hydrophobic guest molecules can be encapsulated. Although possessing a highly ordered structure, in this compound less directional interactions such as van der Waals and hydrophobic effects play important roles. Some nanocubes are reported to exhibit a very high stability beyond the boiling point of water. An MD simulation for the self-assembly process of the nanocube was performed by Harada et al.[65] In their study, by using an enhanced sampling technique instead of the conventional MD simulation, self-assembly process was inferred with the dissociation pathways from the hexameric nanocube form to six monomers in a stepwise manner. They also observed the stability of intermediate oligomers and predicted which process is the rate-determining step during the nanocube formation process. Yamamoto et al. focused on the solvent effect in the molecular level, and computationally examined the self-assembly mechanism in aqueous methanol solution.[66] Starting from the all-atom total free energy calculation and evaluating the aggregation free energy for the partial cluster states, with the use of replica

exchange with solute tempering, it was demonstrated from MD simulations that a highly ordered nanocube structure can be reproduced from the disordered state of the substrates. They also succeeded in offering the insights of the intermediates and encapsulated molecules in the atomistic level. A subsequent study with the newly developed implicit solvent model was performed by Imamura et al. for capturing the nanocube self-assembly process more comprehensively.[67] While it was found that the CG model, which is more advantageous than all-atom model in the calculation efficiency, reasonably explains the solvent effect, the standard CG-MD simulation failed the reproduction of the nanocube structure. On the other hand, replica exchange CG-MD simulation successfully reproduced a highly ordered nanocube structure. Trajectory analysis revealed the transition network, and the main reaction pathways were identified. Finally, although we have focused on the 'self-assembly process' of the nanocube here, it should be noted that Tachikawa et al. also reported the simulation on the same system. In their MD studies, thermodynamic, structural and dynamic properties of the nanocubes and the factors that affect them have been elaborately investigated.[68–71]

One of the most advantageous points in the MD simulation is the visualization of the reaction process, especially the formation of the specific structure in the self-assembly process. MD simulations have also been used in the tracking of the self-organization of virus capsids (one of the simplest examples of the self-assembly in biology), with some ways of simplification and CG being necessary because of the large size.[72] Coordination self-assembly system is more suitable for the MD studies than viral capsids, in that the simpler constituents and the smaller sizes enables the more direct and realistic modeling and unambiguous reaction analysis. However, serious difficulties are still remaining in realizing the time scale of the actual formation of self-assembled structure (second to hour or longer) being very large compared with that accessible in common MD simulations. Some devices and CG procedures are necessary to speed up the simulations.

4 QASAP-NASAP approach

As mentioned in Introduction, the research field of the molecular self-assembly is taking a step from looking only at the objective products under thermodynamic control to actively (kinetically) controlling reaction pathways by modulating the energy landscape. For realizing it in laboratories, it is useful to survey the entire reaction network to capture the information about important events occurring on it, that is, the dominant pathways, the rate-determining step, and kinetic traps and so on. In this section we introduce such attempts, emphasizing the interactive feedback between experimental and computational studies.

4.1 QASAP-NASAP studies

In 2014, Hiraoka and co-workers developed QASAP (quantitative analysis of self-assembly process), a method for clarifying

14664 | Phys. Chem. Chem. Phys., 2023, 25, 14659–14671

This journal is © the Owner Societies 2023

the reaction process of coordination self-assembly consisting of a metal ion M and a multitopic ligand L.[73–75] QASAP was established as an experimental method to follow the reaction process of self-assembling complexes *via* tracking the time evolution of the average composition of the transiently formed intermediates in complex reactions, and has been used to elucidate the reaction process of coordination self-assembly of M_mL_n-type complexes with over 20 different geometric structures.[76–94] Any intermediates of the coordination self-assembly can be indicated by $M_aL_bX_c$ (*a*, *b*, and *c* are 0 or positive integer, and note that the valence of ion is omitted here). QASAP focuses on the following two quantities calculated from *a*, *b*, and *c*,

$$n = \frac{Na - c}{b}, \qquad (5)$$

$$k = \frac{a}{b}. \qquad (6)$$

The *n* value indicates the average number of metal ions M (coordination number *N*) binding to a single multitopic ligand L, while the *k* value indicates the ratio of M against L. In QASAP, all the substrates and products are quantified to obtain time-development of $M_{\langle a \rangle}L_{\langle b \rangle}X_{\langle c \rangle}$, which leads to the $(\langle n \rangle, \langle k \rangle)$ value. Here $\langle \cdot \rangle$ indicates the average of all the intermediates present in the system at each observation time. The self-assembly process can be discussed based on the change in the existence ratios and the $(\langle n \rangle, \langle k \rangle)$ value with time.

The advent of QASAP lifted the research of the molecular self-assembly up to one step higher in that the reaction process became accessible *via* the average composition of intermediate species. Currently this method is being expanded to the systems with other than transition metal ions and multi-step reactions under operative kinetic control. As mentioned above, however, there are limits to what can be obtained from experimental studies alone. NASAP (numerical analysis of self-assembly process) was devised as the other wheel for the coordination self-assembly to complement this deficiency with numerical simulations. NASAP is basically composed of the following procedure: (i) constructing a reaction network from the substrates to the objective products for each target self-assembly system. To what extent the reaction network covers (*i.e.*, how many chemical species and elementary reactions among them are included) is determined from the knowledge of the corresponding experiments. (ii) Assigning a reaction rate constant to each elementary reaction present in the network. In most cases the similar reactions are classified into the same reaction type having the same parameter values, because it is practically impossible to assign different rate constant to each elementary reaction in the case the reaction network is large as in the molecular self-assembly. (iii) Fitting of the simulated results to the experimentally available data by changing (sweeping) the rate constant values in certain specified numerical ranges. For the numerical fitting in which all the elementary reactions are classified into *m* classes, a numerical search in the *m* dimensional parameter space is performed. (iv) Running refined

calculations with the set of rate constant which gives a well-fitted result to the experimental counterpart and obtaining the information of the reaction process such as the time evolution of each molecular species and the number of each reaction that occurred.

Fig. 2 presents a brief overview of the geometrical structures investigated by NASAP studies. Eight self-assembly systems with six geometries have been numerically analysed in detail based on the corresponding QASAP data, though the library of QASAP-NASAP joint research is ongoingly growing with the self-assembly systems larger in the number and more extensive in the diversity. NASAP was originated by Matsumura *et al.*[95] for the analysis of the octahedron-shaped $[Pd_6L_8]^{12+}$ capsule composed of Pd(II) complex and tritopic ligand **1** (Fig. 2(a)),

$$6 \cdot [PdPy_4]^{2+} + 8 \cdot \mathbf{1} \rightarrow [Pd_6\mathbf{1}_8]^{12+} + 12 \text{ Py}. \qquad (7)$$
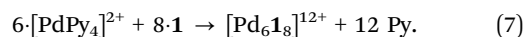
In the corresponding QASAP study,[75] it was possible to quantify all the compounds in eqn (7) due to Py in $[PdPy_4]^{2+}$ being traceable with its ^1H NMR signal.

In this first application of NASAP, parts of the capsule structure ($1 \leq a \leq 6$) were considered as the intermediate species. More than 170 000 structures were categorized based on their composition, and a reaction network of 155 chemical species was constructed. Based on the experimental results that in spite of being the reactant in the final capsule formation ($[Pd_6\mathbf{1}_8Py]^{12+} \rightarrow [Pd_6\mathbf{1}_8Py]^{12+} + Py$) the ^1H NMR of $[Pd_6\mathbf{1}_8Py]^{12+}$ did not appear, two conformational isomers of $[Pd_6\mathbf{1}_8Py]^{12+}$ in slow dynamic equilibrium were explicitly included in their analysis. All the elementary reactions in the network were
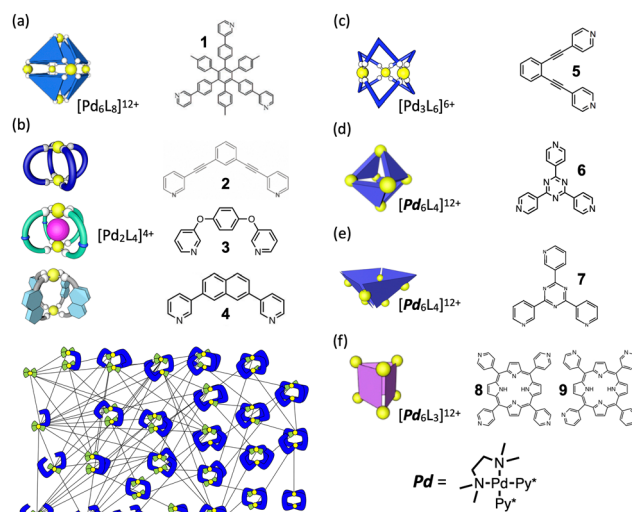

Fig. 2 Geometrical structures of the metal-organic coordination complexes whose self-assembly processes were investigated by NASAP so far. Multitopic ligand used to construct each self-assembly is also indicated. (a) $[Pd_6L_8]^{12+}$ capsule. (b) $[Pd_2L_4]^{4+}$ cages, for which the reaction network employed in the simulations is shown. (c) $[Pd_3L_6]^{6+}$ double-walled triangle. (d) $[Pd_6L_4]^{12+}$ truncated tetrahedron. (e) $[Pd_6L_4]^{12+}$ square-based pyramid. (f) $[Pd_6L_3]^{12+}$ prism. For (d)–(f) self-assemblies, the metal source Pd is *cis*-protected Pd(II) complex (Pd[TMEDA]$^{2+}$) where two coordination sites of the Pd(II) ion are occupied by a chelate ligand (TMEDA: *N,N,N',N'*-tetramethylethylenediamine).

This journal is © the Owner Societies 2023

Phys. Chem. Chem. Phys., 2023, **25**, 14659–14671 | **14665**

classified into four types. They divided the entire self-assembly reaction into three stages and discussed the time evolution of the intermediate species, with the dominant ones being (1) linear oligomers at the initial stage, (2) intramolecular Pd-**1** bonds saturated at the middle stage, and (3) kinetic trapping state at the final stage. The time evolution detected in the corresponding experiment was properly reproduced with the timescale from millisecond to hours.

Motivated by the successful reproduction and analysis of the QASAP result, NASAP has been sophisticated step by step in obtaining the information of the main reaction pathways, the rate-determining step, and the kinetic traps. In the following subsections we show the results of QASAP-NASAP studies.[94]

4.1.1 Pd$_2$L$_4$ cages. From the numerical studies for the following three different Pd$_2$L$_4$ cages explained below (Py* indicates 3-chloropyridine) (Fig. 2(b)),

$$2 \cdot \left[PdPy_4^* \right]^{2+} + 4 \cdot L \rightarrow \left[Pd_2L_4 \right]^{4+} + 8 \cdot Py^*, \qquad (8)$$
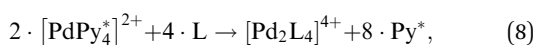
each rate constant was assigned not to the reaction but to the "reaction site" to explicitly distinguish the structural difference (or more specifically, the number of reaction site combination for making a certain structure) among the intermediate species with the same composition. The difference among the self-assembly pathways manifested in the n–k plots of QASAP for three systems was revealed more clearly with the NASAP simulations based on the reaction network as shown in Fig. 2(b).

1. Cage formation with rapid ligand consumption. For the first case, QASAP clearly indicated that the consumption of the ditopic ligand **2** was too fast for the very initial stage of the self-assembly to be unobservable.[78] NASAP was performed for this system with the reaction network having 29 chemical species and 68 elementary reactions among them, each of which has both forward and backward directions.[96] All the elementary reactions were classified into four types based on the similarity of reaction behavior as follows:

1. Intermolecular ligand exchange reaction with a free ligand **2**: k_{1f} [min^{-1} M^{-1}] and k_{1b} [min^{-1} M^{-1}] are defined for the forward and the backward reactions, respectively.

2. Formation of dinuclear species from two mononuclear ones: k_{2f} [min^{-1} M^{-1}] and k_{2b} [min^{-1} M^{-1}] for the forward and the backward, respectively.

3. Intramolecular ligand exchange reaction in dinuclear species: k_{3f} [min^{-1}] and k_{3b} [min^{-1} M^{-1}] for the forward and the backward, respectively.

4. Cage completion: k_{4f} [min^{-1}] and k_{4b} [min^{-1} M^{-1}] for the forward and the backward, respectively.

Rate-determining step was clearly identified as the final stage of the self-assembly (cage completion step). NASAP have also shown the reaction behaviors at the initial stage of the self-assembly, which was not unclear with QASAP alone.

2. Kinetic template effect to avoid sheet formation. In the second application of NASAP to Pd$_2$L$_4$ cage, kinetic template effect of counter anion was confirmed in the self-assembly of ditopic ligand **3** and Pd(II) source [PdPy*$_4$](OTf)$_2$. For this self-assembly, QASAP revealed the reaction pathway was largely affected by the counter anions.[97] Without template anion (NO$_3^-$), a micrometer-sized sheet is kinetically trapped (off-pathway), which is converted into the thermodynamically most stable cage by the template anion. When NO$_3^-$ is present from the start, the cage is selectively produced by the preferential cyclization of a dinuclear intermediate (on-pathway).

For the QASAP results in which the fact that the NO$_3^-$ anion promotes the reactions in the early stage of the self-assembly to a greater extent than those in the final step was extracted, NASAP simulation was conducted with the same reaction network as that used for [Pd$_2$**2**$_4$]$^{4+}$ and a little sophisticated classification of reaction types, in which the intramolecular reaction was separated into two types (the first and the second bridgings). The simulation results were found to support the strong kinetic template effect on the on-pathway, showing that the rate constants of the intramolecular cyclization in the early stage of the self-assembly (k_3 and k_4) are larger than that in the final step (k_5).

3. Navigated self-assembly of Pd$_2$L$_4$ cage with the modulation of energy landscape. In this study, the formation of a thermodynamically metastable [Pd$_2$**4**$_4$]$^{4+}$ cage structure composed of naphthalene-based ditopic ligands (L) and Pd(II) was tracked with both QASAP and NASAP.[98] This is an example of kinetically controlled molecular self-assembly found in a Pd$_2$L$_4$ cage system. In the case without the guest anion (BF$_4^-$) large intermediate species are formed, while with the guest anion the self-assembly proceeds to not the thermodynamically most stable species but a metastable [Pd$_2$**4**$_4$]$^{4+}$ cage, with the anion being encapsulated in it. The self-assembly process to the cage was found to be navigated by the reaction condition with the counter anion BF$_4^-$ in weak coordinative solvent CD$_3$NO$_2$ to modulate energy landscape, with the decomposition into the thermodynamical state being prevented. Also in this case, NASAP with the same setup as for [Pd$_2$**3**$_4$]$^{2+}$ successfully reproduced the corresponding QASAP results and indicated the navigated reaction pathway to the objective structure.

4.1.2 Pd$_3$L$_6$ double-walled triangle (DWT). In the NASAP study for the [Pd$_3$**5**$_6$]$^{6+}$ DWT (double-walled triangle) composed of Pd(II) complexes (Fig. 2(c)), [PdPy*$_4$](BF$_4$)$_2$ and V-shaped ditopic ligand **5**, a much larger chemical reaction network was constructed with 896 elementary reactions connected by 161 species and classified into 9 reaction types (18 rate constant parameters).[99] In molecular self-assemblies which are not the smallest size and whose components are cross-linked with each other, it is very difficult to specify which occurs faster, intermolecular or intramolecular reactions, and/or, bridging or cyclization out of intramolecular reactions. Additionally, another question comes from the ordering of different kinds of intramolecular process and the factors which affect it.

Starting from the numerical reproduction of the corresponding QASAP results,[87] NASAP specified what causes a balance among the participating elementary chemical reactions, that is, oligomerization, double-wall making (*d*) and cyclization (*c*), in the self-assembly process. It was found that the numbers of isomers having the same composition and reaction points available in them and their mutual relations determine the reaction trends

14666 | *Phys. Chem. Chem. Phys.*, 2023, **25**, 14659–14671

This journal is © the Owner Societies 2023

and time ordering in the entire self-assembly process. More specifically, for this Pd₃L₆ DWT system the self-assembly process was found to proceed as *d-c-d-d* after the formation of oligomers with a proper length.

This study is the first example for demonstrating another utility of the network model created in NASAP for predicting experimental results under kinetic conditions. The outcomes of self-assembly depending on the stoichiometric ratio under kinetic control were predicted by numerical simulations with the rate constants fixed by NASAP, which are well consistent with the experimental results in a certain range of the initial stoichiometric ratio of the substrates ($[L]_0/[Pd]_0$), indicating that numerical simulation in a reaction network model is a powerful approach to find an appropriate reaction condition to produce a desired assembly under kinetic control.

4.1.3 Pd₆L₄ systems. As the number of components in the self-assembly increases, there appears more than one geometrical structure being found as the stable products. Competitions between the formation of those structural isomers and branching to the unexpected reaction behaviors from the chemists' intuition are increasingly observed in such self-assemblies. For those cases numerically tracing the self-assembly process was found to be a powerful tool.

1. *Pd₆L₄* truncated tetrahedron. (TT) In this QASAP-NASAP joint study, the self-assembly processes of octahedron-shaped *Pd₆L₄* cages (truncated tetrahedron, TT) consisting of *cis*-protected Pd(ɪɪ) complexes and two kinds of organic tritopic ligands were investigated[100] (Fig. 2(d)). Considering that whether large kinetically trapped species are produced or not is determined by the balance between the oligomerization and the cyclization, the formation of such kinetically trapped species is due to the over oligomerization.

QASAP and NASAP (NASAP is applied to one of the ligands, **6**) indicate that the cyclization is slower than the oligomerization and the cross-linking in the self-assembly of the $[Pd_6 6_4](BF_4)_{12}$ cage. NASAP was performed with the reaction network with 56 chemical species connected with 249 elementary reactions, each of which has the forward and the backward reactions. All the reactions were classified into three types, that is, oligomerization, cyclization, and cross-linking in a formed cycle, for the purpose of describing the process with as small number of parameters to obtain a clear picture as possible. NASAP indicated that the cyclization reactions mainly take place from the linear intermediates and that the relative difference in the rate constants between the oligomerization (k_{oligo}) and the crosslinking ($k_{cross-link}$) does not affect the trend of the self-assembly process of the $[Pd_6 6_4](BF_4)_{12}$ cage. Although a simple comparison between parameter values of the first-order (intramolecular) and the second-order (intermolecular) reactions seems a little too simplistic, this study exemplifies that in some cases many useful insights are accessible even for the not-too-small-sized objective product without too many and complicated classification of elementary reactions.

2. *Pd₆L₄* square-based pyramid (SP). In the QASAP-NASAP joint study for another *Pd₆L₄* structural isomer[101] (Fig. 2(e)), it was confirmed that the self-assembly process is not as simple as can be expected from the final assembly structure and its components. The target is the self-assembly of a *Pd₆7₄* square-based pyramid (SP) composed of six *cis*-protected Pd(ɪɪ) complexes (M) and four triangular tritopic ligands (**7**). A numerical analysis of the experimental data based on a reaction network model where 579 reactions between the possible 112 species were considered revealed the self-assembly pathways to one of the two M₆L₄ isomers, the other of which is the TT isomer as a possible product.

In this study, the intermediate $[Pd_2 7_2 Py^*]^{4+}$, (2,2,1) in a shorthand notation with suffices *a*, *b*, and *c*, was found to be the key species. If (2,2,1) is transformed to (2,2,0) *via* intramolecular reaction, it is a kinetic trap. Intermolecular reaction of (2,2,1) with (2,1,2) lead to the pathway to form (6,4,0) SP. NASAP has also clearly confirmed the main reaction pathway *not* through the expected route from the structure of intermediates.

4.1.4 Pd₆L₃ prism. Although the NASAP study is possible and actually being underway for larger self-assembly systems, coordination self-assembly systems with 6 metal ions are the largest ones reported in the publication. The system introduced here is another example from that group[102] (Fig. 2(f)), though the reaction network is smaller than the double-walled triangle (DWT) due to the metal ion having the coordination number of $N = 2$. The self-assembly process of $[Pd_6 L_3]^{12+}$ coordination prisms consisting of *cis*-protected Pd(ɪɪ) complexes and porphyrin-based tetratopic ligands with four 3-pyridyl or 4-pyridyl groups (L = **8** and **9**) were investigated with both QASAP and NASAP.

From this study, contrary to common intuition, it was found that for both **8** and **9** macrocyclization (*c*) takes faster than bridging reaction (*b*), with the ordering being *c-b-b-b* after oligomerization. Bridging reaction prior to macrocyclization tended to lead to kinetically trapped species, and the relative magnitude of the rate constants between those two kinds of intramolecular reactions was found to be the key factor.

4.2 Comments on the numerical approach used for the kinetic study and related studies

In all the NASAP simulations performed so far, which were introduced in sequence as above, the time evolution of elementary chemical reactions are numerically followed in a stochastic manner, and more specifically, by using the so-called Gillespie algorithm.[103–106] The Gillespie algorithm is one of the kinetic Monte Carlo (kMC) methods, which is implemented from the related stochastic master equation. In the kMC algorithm the time evolution of complex many-particle systems is simulated according to the frequency or transition probability of each event based on the kinetic and procedural information of elementary process and mechanism, through generating random numbers.

This method is widely used in physics, chemistry, biology and engineering. Bortz *et al.* introduced this as a reorganization of the standard Monte Carlo algorithm for the Ising model,[107] in which choices of random configurational transitions are biased according to each transition's likelihood in such a way

This journal is © the Owner Societies 2023

Phys. Chem. Chem. Phys., 2023, **25**, 14659–14671 | **14667**

that transitions which are easy to occur are chosen preferentially. D'orsagna and co-workers simulated and analysed the nucleation and molecular aggregation.[108,109] Comparison with the classic equilibrium equation was shown, and they discussed the differences between them. They indicated the finite-size effect not considered in the mass-balance equation. Master equation approach is also applied to the chemical reactions in gas phase represented by combustion chemistry, with those related to multiple potential wells and connections among them kept in mind.[110,111] Biochemical reactions are also within the scope of successful application of the stochastic method, including single-molecule enzyme,[112] transcriptional regulation,[113] self-assembly of virus capsids,[114] and so on. Battaile shows an application example of the kMC method in engineering, that is, an attempt to reveal a potential mechanism of grain refinement during the deposition of polycrystalline thin films, with careful explanation for the overview of background theory.[115]

In the static kMC method whose examples are listed above, unlike the so-called on-the-fly kMC approaches where possible reaction pathways are produced in a self-developing manner,[116,117] it is necessary to prepare event lists in which all the expected states and reactions are determined in advance and the rates and thermodynamics are obtained from the prepared network. However, this framework enables us to conduct analysis based on the discrete pathway sampling approach, where all the pathways are obtained from geometry optimization, with the post-processing resorting to statistical mechanics and unimolecular rate theory being possible.[118,119]

It is widely known that the chemical reactions represented with the simultaneous equations can be solved (*i.e.*, the time evolution of the molecules supposed to participate in the global chemical reaction can be tracked) by using the ordinary differential equations (ODE). Although we cite only a few references here,[120–122] there is a vast number of articles employing ODE for tracking chemical reactions. The present authors also used the ODE algorithm for tracking the time evolution of a smaller model chemical reactions for the ligand exchange at the very beginning of NASAP project and argued both the similarity and the difference upon the comparison of the numerical results with those from the Gillespie algorithm.[123] For the large molecular numbers as considered in the NASAP studies (QASAP experimental condition) the same reaction behaviors are available, regardless of the computational methods used. The main reason for resorting to the stochastic method in the QASAP-NASAP studies is the countability of both the molecular numbers present in the simulation box and the elementary reactions occurred. While the ODEs only give us a continuous and relatively smooth time evolution of the "concentration" of each intermediate molecule, the stochastic algorithm enables us to know when one of the possible reactions takes place under what circumstances (*i.e.*, distributions of other species). This is one of advantages for the NASAP to analyse and interpret which reaction pathways the particular self-assembly reaction pass through, because a sequence of a simply counting the reaction frequency (occurred number) for each elementary reaction and the corresponding molecular numbers (increase and decrease)

related to that reaction automatically leads to the dominant reaction pathways to the final self-assembly product without the misinterpretation of kinetic traps as the dominant species on the main reaction pathway.

Incidentally, although we refrain listing up all the contributions here in this article, there is a vast number of studies on various kinds of polymerization and supramolecular polymerization reaction with both the stochastic and the deterministic approaches. For the polymerization reaction we cite a review article.[124] And two articles are referred to for the mathematical analysis of supramolecular polymerization,[125,126] in both of which the analysis was performed with both the deterministic and stochastic ways, thereby providing solid ground for their results.

5 Conclusions and outlook

In this perspective article, three approaches were mainly reviewed to unveil the mechanism of self-assembly at the molecular level. One is the semi-quantum chemical Hamiltonian approach to efficiently describe the bond formation of M–L related to the local character of the energy landscape. The second is the molecular dynamics (MD) simulation, which allows to directly track the reaction process. And the third approach is NASAP, a complementary tool for QASAP, to grasp the global aspects of self-assembly. Contributions by the present authors were made mainly for the first and the third approaches, in which theoretical and computational methods were confirmed to play successful roles in understanding and interpreting the self-assembly pathways and inspecting energy landscapes of reaction, from both a local (semi-quantum chemical) and a broader (time evolution of species concentration) points of view. Studies on their lines are extending to the prediction and the presentation of guiding principles for the experimental works related to the topics mentioned below, and those results will be shown elsewhere. It should be noted that most referred researches that are related to the present authors have been performed almost in parallel between experiment and theory. By collaboratively proceeding the research in this way, those studies have been performed successfully with less time lags between them, creating a positive feedback loop. With the knowledge of the energy landscape in hand, it may be possible to make a strategy of skillfully performing the molecular self-assembly under kinetic control.

Finally, we would like to comment on perspectives beyond the thermodynamic treatment for more active control of the system. Many molecular self-assemblies proceed under thermodynamic control based on reversible chemical bonds between components. The main advantage of this is that even if incorrect bonds are formed between components, the reversibility of the bonds allows them to be repaired, and finally the structure which is thermodynamically the most stable is preferred. For this reason, molecular self-assembly in many artificial systems (especially those forming discrete structures) has been conducted with the thermodynamically controlled

14668 | *Phys. Chem. Chem. Phys.*, 2023, **25**, 14659–14671

This journal is © the Owner Societies 2023

condition. Under such a situation, the Boltzmann distribution reflects the free energy difference (ΔG) between products. Since the free energy is a state function, the consequences of self-assembly are independent of the reaction pathway. However, the molecular self-assembly under thermodynamic control is restricted by the Boltzmann distribution and is not almighty, because (1) the thermodynamically most stable products cannot be produced with the yield more than that in the Boltzmann distribution, and (2) metastable species can never be preferentially generated. An example of the limit of the self-assembly under thermodynamic control can be seen in a multicomponent metallo-organic coordination self-assembly consisting of several types of ligands.[127–132] Coordination self-assembly is a topic of increasingly more interest these days. Even in the self-assembly of a relatively simple M_2L_4 cage structure consisting of two M and four L, it is not easy to form specific cage complexes from multiple species of ditopic ligands in a thermodynamically controlled manner.[133] This is because as the number of component types increases, various isomers with close thermodynamic stability are formed, and it is difficult to preferentially produce a single assembly under thermodynamic control.

It has been made clear that in many cases (especially, biological systems) we often observe the kinetically trapped species during self-assembly with a long lifetime.[134–137] This means that nature skillfully uses kinetics by constructing multicomponent assemblies that cannot be constructed under thermodynamic control, through pathway dependence. And it is also possible to find through experimental studies of coordination self-assembly processes that when molecular self-assembly is carried out under certain conditions, the system as a whole exhibits directionality with maintaining locally reversible nature, and that the products are not Boltzmann distributed. These facts indicate that we cannot understand natural phenomena with the simple scheme of reversible bonding being identical to chemical equilibrium, and that there exists a world with irreversibility created from reversible bonding. In such a case we can carry out the molecular self-assembly under kinetic control with pathway selection, and the understanding of the reaction mechanism becomes essential for realizing pathway dependent molecular self-assembly. In the case of molecular self-assembly, however, the relation among the elementary reactions is largely from the textbook reaction and simple polymerization schemes, and necessarily expressed as a form of complex network, with the chemical species and reactions being the nodes and edges, respectively.

Author contributions

Satoshi Takahashi: writing – original draft (equal). Satoru Iuchi: writing – original draft (equal). Shuichi Hiraoka: conceptualization (equal); funding acquisition (equal); project administration (equal); supervision (equal); writing – review & editing (equal). Hirofumi Sato: conceptualization (equal); funding acquisition (equal); project administration (equal); supervision (equal); writing – review & editing (equal).

Conflicts of interest

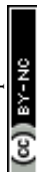There are no conflicts to declare.

Acknowledgements

Notes and references

1 D. J. Kushner, *Bacteriol. Rev.*, 1969, **33**, 302–345.
2 G. M. Whitesides, J. P. Mathias and C. T. Seto, *Science*, 1991, **254**, 1312–1319.
3 G. M. Whitesides and B. Grzybowski, *Science*, 2002, **295**, 2418–2421.
4 S. Zhang, *Nat. Biotechnol.*, 2003, **21**, 1171–1178.
5 A. Tarzia and K. E. Jelfs, *Chem. Commun.*, 2022, **58**, 3717–3730.
6 T. K. Piskorz, V. Martí-Centelles, T. A. Young, P. J. Lusby and F. Duarte, *ACS Catal.*, 2022, **12**, 5806–5826.
7 R. J. Deeth, A. Anastasi, C. Diedrich and K. Randell, *Coord. Chem. Rev.*, 2009, **253**, 795–816.
8 I. Horvath, D. J. Wales and S. N. Fejer, *Nanoscale Adv.*, 2022, **4**, 4272–4278.
9 I. G. Johnston, A. A. Louis and J. P. K. Doye, *J. Phys.: Condens. Matter*, 2010, **22**, 104101.
10 D. J. Wales and T. V. Bogdan, *J. Phys. Chem. B*, 2006, **110**, 20765–20776.
11 D. J. Wales, *Philos. Trans. R. Soc., A*, 2005, **363**, 357–377.
12 D. J. Wales, *Curr. Opin. Struct. Biol.*, 2010, **20**, 3–10.
13 S. Grimme, C. Bannwarth and P. Shushkov, *J. Chem. Theory Comput.*, 2017, **13**, 1989–2009.
14 C. Bannwarth, S. Ehlert and S. Grimme, *J. Chem. Theory Comput.*, 2019, **15**, 1652–1671.
15 B. N. Figgis and M. A. Hitchman, *Ligand Field Theory and Its Applications*, Wiley, New York, 2000.
16 S. Iuchi, A. Morita and S. Kato, *J. Chem. Phys.*, 2004, **121**, 8446–8457.
17 S. Iuchi, *J. Chem. Phys.*, 2012, **136**, 064519.
18 A. V. Soudackov, A. L. Tchougreeff and I. A. Misurkin, *Theor. Chim. Acta*, 1992, **83**, 389–416.
19 A. L. Tchougréeff, A. V. Soudackov, J. van Leusen, P. Kögerler, K.-D. Becker and R. Dronskowski, *Int. J. Quantum Chem.*, 2016, **116**, 282–294.
20 C. E. Schäffer and C. K. Jørgensen, *Mol. Phys.*, 1965, **9**, 401–412.
21 M. B. Darkhovskii and A. L. Tchougréeff, *J. Phys. Chem. A*, 2004, **108**, 6351–6364.
22 I. Popov, E. Plekhanov, A. Tchougréeff and E. Besley, *Mol. Phys.*, 2022, e2106905.
23 P. Li and K. M. Merz Jr., *Chem. Rev.*, 2017, **117**, 1564–1686.

This journal is © the Owner Societies 2023

Phys. Chem. Chem. Phys., 2023, **25**, 14659–14671 | **14669**

24 S. Spicher and S. Grimme, *Angew. Chem., Int. Ed.*, 2020, **59**, 15665–15673.

25 J. G. Brandenburg, C. Bannwarth, A. Hansen and S. Grimme, *J. Chem. Phys.*, 2018, **148**, 064104.

26 S. Spicher, M. Bursch and S. Grimme, *J. Phys. Chem. C*, 2020, **124**, 27529–27541.

27 M. Bursch, H. Neugebauer and S. Grimme, *Angew. Chem., Int. Ed.*, 2019, **58**, 11078–11087.

28 R. J. Deeth and L. J. A. Hearnshaw, *Dalton Trans.*, 2006, 1092–1100.

29 R. J. Deeth, D. L. Foulis and B. J. Williams-Hubbard, *Dalton Trans.*, 2003, 3949–3955.

30 R. J. Deeth, N. Fey and B. Williams-Hubbard, *J. Comput. Chem.*, 2005, **26**, 123–130.

31 P. Melix, F. Paesani and T. Heine, *Adv. Theory Simul.*, 2019, **2**, 1900098.

32 J. Cirera, V. Babin and F. Paesani, *Inorg. Chem.*, 2014, **53**, 11020–11028.

33 C. E. Schäffer, C. Anthon and J. Bendix, *Coord. Chem. Rev.*, 2009, **253**, 575–593.

34 S. K. Singh, J. Eng, M. Atanasov and F. Neese, *Coord. Chem. Rev.*, 2017, **344**, 2–25.

35 L. Lang, M. Atanasov and F. Neese, *J. Phys. Chem. A*, 2020, **124**, 1025–1037.

36 M. Buchhorn, R. J. Deeth and V. Krewald, *Chem. – Eur. J.*, 2022, **28**, e202103775.

37 Y. Matsumura, S. Iuchi and H. Sato, *Phys. Chem. Chem. Phys.*, 2018, **20**, 1164–1172.

38 Y. Matsumura, S. Iuchi, S. Hiraoka and H. Sato, *Phys. Chem. Chem. Phys.*, 2018, **20**, 7383–7386.

39 Y. Yoshida, S. Iuchi and H. Sato, *Phys. Chem. Chem. Phys.*, 2021, **23**, 866–877.

40 D. J. Wales, *Annu. Rev. Phys. Chem.*, 2018, **69**, 401–425.

41 D. J. Wales, *J. Chem. Phys.*, 2015, **142**, 130901.

42 F. Noé and S. Fischer, *Curr. Opin. Struct. Biol.*, 2008, **18**, 154–162.

43 D. Prada-Gracia, J. Gómez-Gardeñes, P. Echenique and F. Fernando, *PLoS Comput. Biol.*, 2009, **5**, e1000415.

44 O. M. Becker and M. Karplus, *J. Chem. Phys.*, 1997, **106**, 1495–1517.

45 D. J. Wales, M. A. Miller and T. R. Walsh, *Nature*, 1998, **394**, 758–760.

46 F. Calvo, J. P. K. Doye and D. J. Wales, *Nanoscale*, 2012, **4**, 1085–1100.

47 D. Schebarchov, F. Baletto and D. J. Wales, *Nanoscale*, 2018, **10**, 2004–2016.

48 J. Hernández-Rojas, F. Calvo, S. Niblett and D. J. Wales, *Phys. Chem. Chem. Phys.*, 2017, **19**, 1884–1895.

49 J. D. Farrell, C. Lines, J. J. Shepherd, D. Chakrabarti, M. A. Miller and D. J. Wales, *Soft Matter*, 2013, **9**, 5407–5416.

50 Y. Yoshida, H. Sato, J. W. R. Morgan and D. J. Wales, *Chem. Phys. Lett.*, 2016, **664**, 5–9.

51 J. W. R. Morgan, D. Mehta and D. J. Wales, *Phys. Chem. Chem. Phys.*, 2017, **19**, 25498–25508.

52 J. A. Joseph, K. Röder, D. Chakraborty, R. G. Mantell and D. J. Wales, *Chem. Commun.*, 2017, **53**, 6974–6988.

53 J. M. Carr and D. J. Wales, *Phys. Chem. Chem. Phys.*, 2009, **11**, 3341–3354.

54 B. Barz, D. J. Wales and B. Strodel, *J. Phys. Chem. B*, 2014, **118**, 1003–1011.

55 J. D. Stevenson and D. J. Wales, *J. Chem. Phys.*, 2014, **141**, 041104.

56 D. J. Sharpe and D. J. Wales, *J. Chem. Phys.*, 2019, **151**, 124101.

57 T. D. Swinburne and D. J. Wales, *J. Chem. Theory Comput.*, 2020, **16**, 2661–2679.

58 M. Yoneya, S. Tsuzuki, T. Yamaguchi, S. Sato and M. Fujita, *ACS Nano*, 2014, **8**, 1290–1296.

59 M. Yoneya, T. Yamaguchi, S. Sato and M. Fujita, *J. Am. Chem. Soc.*, 2012, **134**, 14401–14407.

60 A. V. Zhukhovitskiy, M. Zhong, E. G. Keeler, V. K. Michaelis, J. E. P. Sun, M. J. A. Hore, D. J. Pochan, R. G. Griffin, A. P. Willard and J. A. Johnson, *Nat. Chem.*, 2016, **8**, 33–41.

61 Y. Jiang, H. Zhang, Z. Cui and T. Tan, *J. Phys. Chem. Lett.*, 2017, **8**, 2082–2086.

62 M. Yoneya, S. Tsuzuki and M. Aoyagi, *Phys. Chem. Chem. Phys.*, 2015, **17**, 8649–8652.

63 D. Biswal and P. G. Kusalik, *ACS Nano*, 2017, **11**, 258–268.

64 D. Biswal and P. G. Kusalik, *J. Chem. Phys.*, 2017, **147**, 044702.

65 R. Harada, T. Mashiko, M. Tachikawa, S. Hiraoka and Y. Shigeta, *Phys. Chem. Chem. Phys.*, 2018, **20**, 9115–9122.

66 T. Yamamoto, H. Are, S. Shanker, H. Sato and S. Hiraoka, *J. Phys. Chem. Lett.*, 2018, **9**, 6082–6088.

67 K. Imamura, T. Yamamoto and H. Sato, *Chem. Phys. Lett.*, 2020, **742**, 137135.

68 J. Koseki, Y. Kita, S. Hiraoka, U. Nagashima and M. Tachikawa, *Int. J. Quantum Chem.*, 2013, **113**, 397–400.

69 T. Mashiko, K. Yamada, T. Kojima, S. Hiraoka, U. Nagashima and M. Tachikawa, *Chem. Lett.*, 2014, **43**, 366–368.

70 T. Mashiko, K. Yamada, S. Hiraoka, U. Nagashima and M. Tachikawa, *Mol. Simul.*, 2015, **41**, 845–849.

71 T. Mashiko, S. Hiraoka, U. Nagashima and M. Tachikawa, *J. Phys. Chem. B*, 2019, **123**, 5176–5180.

72 D. C. Rapaport, *Phys. Biol.*, 2010, **7**, 045001.

73 A. Baba, T. Kojima and S. Hiraoka, *J. Am. Chem. Soc.*, 2015, **137**, 7664–7667.

74 A. Baba, T. Kojima and S. Hiraoka, *Chem. – Eur. J.*, 2018, **24**, 838–847.

75 Y. Tsujimoto, T. Kojima and S. Hiraoka, *Chem. Sci.*, 2014, **5**, 4167–4172.

76 S. Kai, Y. Sakuma, T. Mashiko, T. Kojima, M. Tachikawa and S. Hiraoka, *Inorg. Chem.*, 2017, **56**, 12652–12663.

77 S. Kai, T. Shigeta, T. Kojima and S. Hiraoka, *Chem. – Asian J.*, 2017, **12**, 3203–3207.

78 S. Kai, V. Marti-Centelles, Y. Sakuma, T. Mashiko, T. Kojima, U. Nagashima, M. Tachikawa, P. J. Lusby and S. Hiraoka, *Chem. – Eur. J.*, 2018, **24**, 663–671.

79 A. Baba, T. Kojima and S. Hiraoka, *Chem. – Eur. J.*, 2018, **24**, 838–847.

14670 | *Phys. Chem. Chem. Phys.*, 2023, **25**, 14659–14671

This journal is © the Owner Societies 2023

80 S. Kai, M. Nakagawa, T. Kojima, X. Li, M. Yamashina, M. Yoshizawa and S. Hiraoka, *Chem. – Eur. J.*, 2018, **24**, 3965–3969.

81 T. Tateishi, W. Zhu, L. H. Foianesi-Takeshige, T. Kojima, K. Ogata and S. Hiraoka, *Eur. J. Inorg. Chem.*, 2018, 1192–1197.

82 T. Tateishi, T. Kojima and S. Hiraoka, *Inorg. Chem.*, 2018, **57**, 2686–2694.

83 S. Kai, S. P. Maddala, T. Kojima, S. Akagi, K. Harano, E. Nakamura and S. Hiraoka, *Dalton Trans.*, 2018, **47**, 3258–3263.

84 T. Tateishi, T. Kojima and S. Hiraoka, *Commun. Chem.*, 2018, **1**, 20.

85 S. Kai, T. Kojima, F. L. Thorp-Greenwood, M. J. Hardie and S. Hiraoka, *Chem. Sci.*, 2018, **9**, 4104–4108.

86 M. Nakagawa, S. Kai, T. Kojima and S. Hiraoka, *Chem. – Eur. J.*, 2018, **24**, 8804–8808.

87 T. Tateishi, S. Kai, Y. Sasaki, T. Kojima, S. Takahashi and S. Hiraoka, *Chem. Commun.*, 2018, **54**, 7758–7761.

88 S. Kai, T. Tateishi, T. Kojima, S. Takahashi and S. Hiraoka, *Inorg. Chem.*, 2018, **57**, 13083–13086.

89 S. Hiraoka, *Isr. J. Chem.*, 2019, **59**, 151–165.

90 S. Komine, T. Tateishi, T. Kojima, H. Nakagawa, Y. Hayashi, S. Takahashi and S. Hiraoka, *Dalton Trans.*, 2019, **48**, 4139–4148.

91 T. Tateishi, Y. Yasutake, T. Kojima, S. Takahashi and S. Hiraoka, *Commun. Chem.*, 2019, **2**, 25.

92 S. Hiraoka, *Chem. Rec.*, 2015, **15**, 1144–1147.

93 S. Hiraoka, *Bull. Chem. Soc. Jpn.*, 2018, **91**, 957–978.

94 S. Hiraoka, S. Takahashi and H. Sato, *Chem. Rec.*, 2021, **21**, 443–459.

95 Y. Matsumura, S. Hiraoka and H. Sato, *Phys. Chem. Chem. Phys.*, 2017, **19**, 20338–20342.

96 S. Takahashi, Y. Sasaki, S. Hiraoka and S. Sato, *Phys. Chem. Chem. Phys.*, 2019, **21**, 6341–6347.

97 L. H. Foianesi-Takeshige, S. Takahashi, T. Tateishi, R. Sekine, A. Okazawa, W. Zhu, T. Kojima, K. Harano, E. Nakamura, H. Sato and S. Hiraoka, *Commun. Chem.*, 2019, **2**, 128.

98 T. Tateishi, S. Takahashi, A. Okazawa, V. Martí-Centelles, J. Wang, T. Kojima, P. J. Lusby, H. Sato and S. Hiraoka, *J. Am. Chem. Soc.*, 2019, **141**, 19669–19676.

99 S. Takahashi, T. Tateishi, Y. Sasaki, H. Sato and S. Hiraoka, *Phys. Chem. Chem. Phys.*, 2020, **22**, 26614–26626.

100 S. Komine, S. Takahashi, T. Kojima, H. Sato and S. Hiraoka, *J. Am. Chem. Soc.*, 2019, **141**, 3178–3186.

101 T. Tateishi, S. Takahashi, I. Kikuchi, K. Aratsu, H. Sato and S. Hiraoka, *Inorg. Chem.*, 2021, **60**, 16678–16685.

102 X. Zhang, S. Takahashi, K. Aratsu, I. Kikuchi, H. Sato and S. Hiraoka, *Phys. Chem. Chem. Phys.*, 2022, **24**, 2997–3006.

103 D. T. Gillespie, *J. Comput. Phys.*, 1976, **22**, 403–434.

104 D. T. Gillespie, *J. Phys. Chem.*, 1977, **81**, 2340–2361.

105 D. T. Gillespie, *Phys. A*, 1992, **188**, 404–425.

106 D. T. Gillespie, *Annu. Rev. Phys. Chem.*, 2007, **58**, 35–55.

107 A. B. Bortz, M. H. Kalos and J. L. Lebowitz, *J. Comput. Phys.*, 1975, **17**, 10–18.

108 M. R. D'Orsogna, G. Lakatos and T. Chou, *J. Chem. Phys.*, 2012, **136**, 084110.

109 M. R. D'Orsogna, B. Zhao, B. Berenji and T. Chou, *J. Chem. Phys.*, 2013, **139**, 121918.

110 J. A. Miller and S. J. Klippenstein, *J. Phys. Chem. A*, 2006, **110**, 10528–10544.

111 M. J. Pilling and S. H. Robertson, *Annu. Rev. Phys. Chem.*, 2003, **54**, 245–275.

112 H. Qian and L. M. Bishop, *Int. J. Mol. Sci.*, 2010, **11**, 3472–3500.

113 T. B. Kepler and T. C. Elston, *Biophys. J.*, 2001, **81**, 3116–3136.

114 B. Sweeney, T. Zhang and R. Schwartz, *Biophys. J.*, 2008, **94**, 772–783.

115 C. C. Battaile, *Comput. Methods Appl. Mech. Engrg.*, 2008, **197**, 3386–3398.

116 H. Xu, Y. N. Osetsky and R. E. Stoller, *Phys. Rev. B: Condens. Matter Mater. Phys.*, 2011, **84**, 132103.

117 X. Guo, D. Minakata and J. Crittenden, *Environ. Sci. Technol.*, 2015, **49**, 9230–9236.

118 D. J. Wales, *Mol. Phys.*, 2002, **100**, 3285–3305.

119 D. J. Wales, *Int. Rev. Phys. Chem.*, 2006, **25**, 237–282.

120 R. E. Glaser, M. A. Delarosa, A. O. Salau and C. Chicone, *J. Chem. Educ.*, 2014, **91**, 7.

121 W. S. Hlavacek, A. Redondo, C. Wofsy and B. Goldstein, *Bull. Math. Biol.*, 2002, **64**, 887–911.

122 P. Moisant, H. Neeman and A. Zlotnick, *Biophys. J.*, 2010, **99**, 1350–1357.

123 T. Iioka, S. Takahashi, Y. Yoshida, Y. Matsumura, S. Hiraoka and S. Sato, *J. Comput. Chem.*, 2019, **40**, 279–285.

124 E. Saldívar-Guerra, *Macromol. React. Eng.*, 2020, **14**, 2000010.

125 A. J. Markvoort, H. M. M. ten Eikelder, P. A. J. Hilbers, T. F. A. de Greef and E. W. Meijer, *Nat. Commun.*, 2011, **2**, 509.

126 A. J. Markvoort, H. M. M. ten Eikelder, P. A. J. Hilbers and T. F. A. de Greef, *ACS Cent. Sci.*, 2016, **2**, 232–241.

127 W. M. Bloch, Y. Abe, J. J. Holstein, C. M. Wandtke, B. Dittrich and G. H. Clever, *J. Am. Chem. Soc.*, 2016, **138**, 13750–13755.

128 J. E. M. Lewis, A. Tarzia, A. J. P. White and K. E. Jelfs, *Chem. Sci.*, 2020, **11**, 677–683.

129 R.-J. Li, J. Tessarolo, H. Lee and G. H. Clever, *J. Am. Chem. Soc.*, 2021, **143**, 3865–3873.

130 D. Preston, J. E. Barnsley, K. C. Gordon and J. D. Crowley, *J. Am. Chem. Soc.*, 2016, **138**, 10578–10585.

131 H. Yu, J. Li, C. Shan, T. Lu, X. Jiang, J. Shi, L. Wojtas, H. Zhang and M. Wang, *Angew. Chem., Int. Ed.*, 2021, **60**, 26523–26527.

132 Y.-Q. Zou, D. Zhang, T. K. Ronson, A. Tarzia, Z. Lu, K. E. Jelfs and J. R. Nitschke, *J. Am. Chem. Soc.*, 2021, **143**, 9009–9015.

133 S. Pullen, J. Tessarolo and G. H. Clever, *Chem. Sci.*, 2021, **12**, 7269–7293.

134 J. B. Lingrel and T. Kuntzweiler, *J. Biol. Chem.*, 1994, **269**, 19659–19662.

135 J. H. Kaplan, *Annu. Rev. Biochem.*, 2002, **71**, 511–535.

136 C. M. Dobson, A. Šali and M. Karplus, *Angew. Chem., Int. Ed.*, 1998, **37**, 868–893.

137 G. M. Whitesides and R. F. Ismagilov, *Science*, 1999, **284**, 89–92.

This journal is © the Owner Societies 2023

Phys. Chem. Chem. Phys., 2023, **25**, 14659–14671 | **14671**